



OPEN ACCESS

EDITED BY
Matheus Mattos,
KU Leuven, Belgium

REVIEWED BY
Zhang Xiaowei,
Henan University of Chinese Medicine, China
Yingying Yu,
Hangzhou University, China
Yifeng Zheng,
National Fisheries University, Japan

*CORRESPONDENCE

Xing Li
✉ lixing530@zzu.edu.cn
Hanlu Song
✉ shanlu9810@163.com
Lili Lang
✉ langlili@czmc.cn

RECEIVED 10 May 2025

ACCEPTED 27 June 2025

PUBLISHED 17 July 2025

CITATION

Miao Y, Zhang Y, Zhang L, Chen H, Tang L,
Li W, Gu C, Lang L, Li X and Song H (2025)
Vitamin D ameliorates prediabetic cardiac
injury via modulation of the ErbB4/
ferroptosis signaling axis.
Front. Immunol. 16:1626295.
doi: 10.3389/fimmu.2025.1626295

COPYRIGHT

© 2025 Miao, Zhang, Zhang, Chen, Tang, Li,
Gu, Lang, Li and Song. This is an open-access
article distributed under the terms of the
[Creative Commons Attribution License \(CC BY\)](#).
The use, distribution or reproduction in other
forums is permitted, provided the original
author(s) and the copyright owner(s) are
credited and that the original publication in
this journal is cited, in accordance with
accepted academic practice. No use,
distribution or reproduction is permitted
which does not comply with these terms.

Vitamin D ameliorates prediabetic cardiac injury via modulation of the ErbB4/ferroptosis signaling axis

Yufan Miao¹, Yujing Zhang¹, Luoya Zhang¹, Hao Chen¹,
Lulu Tang¹, Wenjie Li¹, Chenxi Gu², Lili Lang^{3*}, Xing Li^{1,4*}
and Hanlu Song^{1,5*}

¹Department of Nutrition and Food Hygiene, College of Public Health, Zhengzhou University, Zhengzhou, Henan, China, ²Department of Orthopedics, The First Affiliated Hospital of Zhengzhou University, Zhengzhou, Henan, China, ³Biomedical Engineering Department, Changzhi Medical College, Changzhi, Shanxi, China, ⁴Department of Hematology, The First Affiliated Hospital of Zhengzhou University, Zhengzhou, Henan, China, ⁵School of Design and Innovation, Tan Kah Kee College, Xiamen University, Zhangzhou, China

Vitamin D (VD) deficiency is closely associated with metabolic health and cardiac function in prediabetic patients, yet its underlying mechanisms remain unclear. This study investigated the role of VD intervention in prediabetic cardiac injury through *in vivo* and *in vitro* models, with particular focus on the ErbB4/ferroptosis axis. Using a high-fat diet-induced KKAY prediabetic mouse model, we observed significant metabolic abnormalities (increased body weight, hyperglycemia, insulin resistance) and cardiac remodeling (cardiac hypertrophy and functional impairment) ($P < 0.05$). Remarkably, 16-week vitamin D (VD₃) supplementation substantially ameliorated these pathological changes and reduced serum cardiac injury markers ($P < 0.05$). Mechanistic studies revealed that VD₃ downregulated myocardial NRG1 expression, inhibited ErbB4 phosphorylation (p-ErbB4) and YAP activation (p-YAP), while reversing the abnormal expression of ferroptosis-related proteins. *In vitro* experiments confirmed that high glucose combined with palmitic acid (HGPA) induced ferroptosis in H9c2 cardiomyocytes, which was alleviated by 1,25(OH)₂D₃ intervention through suppression of ErbB4 phosphorylation. Notably, combined treatment with 1,25(OH)₂D₃ and the ErbB4 phosphorylation inhibitor dacomitinib demonstrated synergistic protective effects. Our findings not only expand the understanding of the association between prediabetes and VD, but also reveal a relationship between ErbB4 and cardiac ferroptosis in prediabetic conditions.

KEYWORDS

prediabetes, vitamin D, ErbB4, ferroptosis, myocardial injury

1 Introduction

Cardiovascular complications represent a major cause of morbidity and mortality in diabetic patients, with cardiac dysfunction emerging as a particularly devastating consequence of chronic metabolic dysregulation (1). The pathophysiological triad of hyperglycemia, insulin resistance, and compensatory hyperinsulinemia creates a vicious cycle that progressively impairs cardiac function, ultimately culminating in structural abnormalities including myocardial hypertrophy, fibrosis, and both diastolic and systolic dysfunction (2, 3). Despite the clinical significance of diabetic cardiomyopathy, current therapeutic options remain limited, highlighting the urgent need for novel intervention strategies.

Emerging evidence suggests that the path to diabetic heart failure may begin during the prediabetic stage, characterized by early manifestations of left ventricular hypertrophy and diastolic dysfunction (4, 5). This preclinical phase represents a critical therapeutic window, as metabolic and cardiac abnormalities at this stage may still be reversible through timely intervention, in contrast to the largely irreversible damage observed in established diabetes. Among potential interventions, vitamin D (VD) has attracted considerable attention due to its pleiotropic effects on glucose metabolism and cardiovascular function (6–8). Epidemiologic studies have demonstrated that VD supplementation can reduce the risk of diabetes progression in prediabetic individuals by up to 46%, while mechanistic research has revealed multiple cardioprotective pathways mediated through the vitamin D receptor (VDR) (9–11). However, the specific benefits of VD intervention during the prediabetic phase, particularly regarding early cardiac protection, remain poorly understood.

At the cellular level, the pathogenesis of diabetic cardiomyopathy involves complex interactions between metabolic stress and oxidative damage (12). The diabetic milieu, characterized by chronic hyperglycemia and hyperlipidemia, promotes excessive generation of reactive oxygen species (ROS) and lipid peroxides, creating conditions conducive to ferroptosis - an iron-dependent form of regulated cell death that may play a pivotal role in myocardial injury (12–14). Interestingly, recent studies have implicated the epidermal growth factor receptor ErbB4 as a potential mediator between metabolic stress and cardiomyocyte survival (15, 16). While the NRG1/ErbB4 signaling axis is known to regulate cardiac remodeling, and high glucose conditions have been shown to upregulate NRG1 expression, the potential crosstalk between ErbB4 signaling and ferroptosis in the diabetic heart remains unexplored (15, 17–19).

To address these critical questions, we employed a comprehensive experimental approach combining *in vivo* and *in vitro* models of prediabetic cardiac injury. Using high fat diet (HFD) -fed KKAY mice and high glucose/palmitic acid (HGPA)-treated H9c2 cardiomyocytes, we systematically investigated (1): the cardioprotective effects of VD intervention during the prediabetic stage; (2) the involvement of ErbB4 signaling in metabolic stress-induced cardiac injury; and (3) the potential interplay between ErbB4 activation and ferroptosis regulation in the diabetic heart. Our findings provide novel insights into the molecular mechanisms underlying early diabetic cardiomyopathy and identify potential targets for preventive intervention.

2 Materials and methods

2.1 Chemical reagents and antibodies

VD₃ was procured from Sigma Aldrich (St. Louis, MO, USA). Dulbecco's modified eagle medium (DMEM) and fetal bovine serum (FBS) were obtained from GIBCO (Grand Island, NY, USA) and LONSERA (Auckland, New Zealand), respectively. 1,25 (OH)₂D₃ and Ferrostatin-1 (Fer-1) were purchased from GLPBIO (Montclair, CA, USA), and Dacomitinib (Dac) was acquired from MedChemExpress (Monmouth Junction, NJ, USA). The sources of antibodies were as follows: NRG1 (10527-1-AP), SLC7A11 (26864-1-AP), TFR1 (84766-4-RR), NCOA4 (83394-4-RR), β -actin (20536-1-AP) were purchased from Proteintech (Wuhan, China), ErbB4 (RT1276), YAP (RT1664), Phospho-YAP (ET1611-69), ACSL4 (ET7111-43), Ferritin (R1601-9), GPX4 (ET1706-45) were purchased from HUABIO (Hangzhou, China). Phospho-ErbB4 (Tyr1284) (AF3445) were purchased from Affinity Biosciences (Cincinnati, USA).

2.2 Animals and Grouping

Four-week-old specific pathogen free (SPF) male C57BL/6J mice (n=12) and KKAY mice (n=48) were purchased from Beijing Huafukang Bio-technology Co. The animals were housed in a controlled barrier facility with a 12h light/dark cycle at 22 \pm 1°C and 55 \pm 5% humidity, with ad libitum access to food and water. Following a 2-week acclimatization period, C57BL/6J mice were designated as the normal control group (NC) and fed a standard chow diet (fat: 4.0 gm%), while KKAY mice received a HFD (17.9 gm%) for 6 weeks to establish a prediabetic model. The modeling criteria were defined as fasting blood glucose (FBG) levels maintained within 6.7 to 16.7 mmol/L, combined with 2h post-oral glucose tolerance test (2h-OGTT) blood glucose levels ranging from 11.1 to 30 mmol/L. Successfully modeled KKAY mice were randomly divided into four groups according to body weight and FBG levels: model group (MC), low-dose VD₃ intervention group (LVD, 0.42 IU/g/w), medium-dose VD₃ intervention group (MVD, 1.68 IU/g/w), and high-dose VD₃ intervention group (HVD, 4.20 IU/g/w). VD₃ dissolved in 0.1 mL corn oil was administered via intraperitoneal injection, and the NC and MC groups received an equivalent volume of corn oil. After 16 weeks of VD₃ intervention, mice were anesthetized by intraperitoneal injection of sodium pentobarbital at a dose of 50 mg/kg. Heart tissues and blood samples were then immediately collected and preserved for further analysis. All animal experiments were approved by the Life Sciences Ethics Review Committee of Zhengzhou University (Ethics No. ZZUIRB2021-GZR0141).

2.3 Echocardiographic measurement

After 16 weeks of VD₃ intervention, echocardiography was performed by using Vevo2100 imaging system. Parasternal short-

axis M-mode echocardiographic images were obtained at papillary muscles level. The following parameters were recorded: left ventricular (LV) mass, left ventricular volume at diastole and systole (LV Vol;d and LV Vol;s), left ventricular internal dimension at diastole and systole (LVID;d and LVID;s), left ventricular ejection fraction (EF), fractional shortening (FS), and interventricular septal thickness at systole and diastole (IVS;s and IVS;d).

2.4 Biochemical analysis

FBG, total cholesterol (TC), low-density and high-density lipoprotein cholesterol (LDL-C and HDL-C), creatine kinase (CK) and lactate dehydrogenase (LDH) levels were measured using the Nanjing JianCheng Assay Kits. Serum fasting insulin (INS) and 25(OH)D were measured using Mlbio Enzyme-linked immunosorbent assay Kits.

2.5 Measurement of tissue iron, glutathione and malondialdehyde levels

Heart tissue (50 mg) was precisely weighed and placed into a grinding tube containing grinding beads. Subsequently, 450 mL of physiological saline was added, and the tissue was thoroughly ground using a grinder. The resulting mixture was then centrifuged in a pre-cooled centrifuge for 10 min, after which the supernatant was collected for measurement. The protein concentration was determined, and Fe, GSH, and MDA levels were measured as per the provided instructions. Subsequently, values were calculated and analyzed using the designated formulas.

2.6 Hematoxylin & eosin, wheat germ agglutinin and Perls prussian blue with DAB staining

Following fixation in 4% paraformaldehyde, cardiac tissues were sequentially subjected to graded ethanol dehydration, xylene clearing, paraffin infiltration, and sectioning into 3–5 μ m slices using a rotary microtome. For histological analysis, sections were dewaxed in xylene (3 \times 5 min), rehydrated through descending ethanol gradients (100%, 95%, 75%; 2 min each), and stained with H&E per standard protocols. For WGA staining, the sections underwent dewaxing, antigen retrieval, and incubation with primary and secondary antibodies. Simultaneously, the WGA working solution was drop-stained, counterstained with DAPI for nuclear localization, and imaged under a laser scanning confocal microscope. The cross-sectional area of cardiomyocytes was measured using Image J software, and the resulting data were analyzed. Furthermore, sections were deparaffinized, stained with Prussian blue and DAB, and images were observed and captured using a light microscope.

2.7 Oil red O and ROS staining

The tissues preserved at -80°C were embedded using OCT compound to prepare frozen sections. Subsequently, these sections were stained with oil red O following the provided guidelines, and the resulting images were observed and captured using a light microscope. For further analysis, the frozen sections were allowed to thaw to room temperature, ensuring moisture control and subsequent drying. Tissue autofluorescence was minimized, and a staining solution for ROS was meticulously added to the sections. After restaining the nuclei with DAPI, the sections were sealed and observed using fluorescence microscopy, with images captured for subsequent analysis.

2.8 TUNEL staining

Cardiac paraffin sections were deparaffinized in xylene (3 \times 10 min) and rehydrated through a graded ethanol series into distilled water. Antigen retrieval was performed in citrate buffer at 95°C for 20 min. After cooling to room temperature, sections were washed in PBS (3 \times 5 min), permeabilized with 0.1% Triton X-100 for 10 min, and treated in 3% hydrogen peroxide in methanol for 20 min in the dark. To suppress lipofuscin autofluorescence, sections were incubated with 10% acetic acid in methanol for 10 min and rinsed in PBS (3 \times 5 min). Following equilibration in commercial equilibration buffer, sections were incubated with TUNEL reaction mixture at 37°C for 90 min in a humidified dark chamber. After washing in stop/wash buffer (3 \times 10 min), Converter-POD was applied for 30 min at 37°C . DAB chromogen was used for signal development under microscopic monitoring. Sections were counterstained with Mayer's hematoxylin for 45 sec, dehydrated through graded ethanol, cleared in xylene, and mounted with DPX mounting medium.

2.9 Cell cultures and treatment

H9c2 cells were obtained from the First Affiliated Hospital of Zhengzhou University and cultured in DMEM medium supplemented with 10% FBS and 1% penicillin/streptomycin at 37°C in humidified 5% CO_2 conditions. The cells were used in the experiments once they reached 70–80% confluence. High glucose and palmitic acid medium (HGPA, 33.3 mM d-glucose, 0.25 mM PA) was used to construct injury models by culturing cells for 24h. Addition of 10 nM $1,25(\text{OH})_2\text{D}_3$ and/or 73.7 nM Dacomitinib or 1 μM Ferrostatin-1 pretreated the cells for 2h while co-culturing the cells with HGPA for 24h (Figure 1).

2.10 Cell viability assay

Cells were seeded in 96-well plates, allowing them to adhere before the addition of medium containing various concentrations of

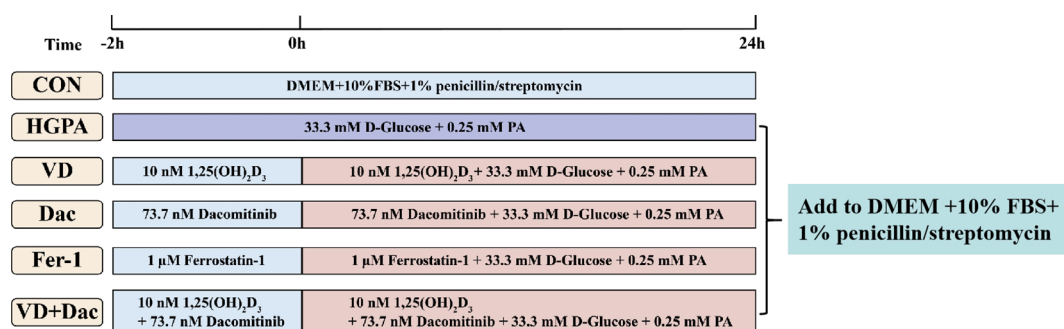


FIGURE 1
Experimental design of cell experiments.

intervening substances. Subsequently, 10 μ L of Cell Counting Kit-8 (ApexBio, Houston, USA) solution was introduced into each well, and the plates were incubated at 37°C in an incubator for 1–4 h. Absorbance at 450 nm was measured, and cell viability was calculated based on the recorded measurements.

2.11 Detection of ROS in cells

Add a minimum of 1 mL of 10 μ M DCFH-DA to the cultured cells, enabling its free passage through the cell membrane. Subsequently, intracellular lipase hydrolyzes DCFH-DA into DCFH, which is unable to traverse the cell membrane. Active oxygen within the cell oxidizes DCFH to form DCF, which exhibits fluorescence. The fluorescence intensity of DCF serves as an indicator to measure intracellular active oxygen levels. Incubate the cells for 20 minutes at 37°C in the cell incubator to facilitate the process. Remove any residual DCFH-DA that hasn't entered the cells, then observe and capture images using a fluorescence microscope.

2.12 Western blot analysis

Proteins extracted from murine hearts and cells were initially separated using SDS-PAGE gel and subsequently transferred onto polyvinylidene fluoride membranes. Following this, the membranes were blocked using either 5% skim milk or bovine serum albumin. Later, they underwent incubation with primary and secondary antibodies and were detected using an ECL detection system.

2.13 Statistical analysis

The obtained results underwent statistical analysis via SPSS 25.0 software. For quantitative data, normality and tests for normality and variance homogeneity were performed. Quantitative data were presented as mean \pm standard deviation (Mean \pm SD). Between-group comparisons were performed using ANOVA for one-way multilevel quantitative data and ANOVA for repeated measures

across multiple time points. Additionally, the Tukey's HSD was employed for two-way comparisons between groups, $P < 0.05$ was considered statistically significant.

3 Result

3.1 VD₃ supplementation ameliorates VD deficiency and glucolipid metabolism disorders in prediabetic mice

Basic index analysis showed that compared with the C57BL/6J control group (NC group), KKAY mice showed remarkable metabolic abnormalities ($P < 0.01$), including: accelerated body weight gain (Figure 2A), decreased serum 25(OH)D concentrations (Figure 2B), elevated FBG levels (Figure 2C), impaired glucose tolerance (Figures 2D–F), hyperinsulinemia evidenced by increased fasting insulin and HOMA-IR (Figures 2G, H), and dyslipidemia manifested by altered TC, LDL-C, and HDL-C levels (Figures 2J–L). Notably, 16-week VD₃ supplementation significantly ameliorated all these metabolic abnormalities except for body weight and HDL-C changes ($P < 0.01$).

3.2 VD₃ supplementation preserves cardiac structure and function in prediabetic mice

Compared with the NC group, MC group mice exhibited significant cardiac remodeling ($P < 0.01$), characterized by increased heart weight, cardiomyocyte hypertrophy, and marked disorganization of myocardial fibers with prominent vacuolization (Figures 3A, B). Echocardiographic assessment confirmed severe cardiac dysfunction in MC mice ($P < 0.01$), demonstrating elevated LV mass (Figure 3C), increased end-diastolic and end-systolic LV volumes (LV Vol;d and LV Vol;s) (Figures 3E, F), and enlarged LV internal diameters during both diastole and systole (LVID;d and LVID;s) (Figures 3G, H). Concurrently, systolic function was significantly impaired, as evidenced by reduced ejection fraction (EF%) and fractional shortening (FS%) (Figures 3I, J) ($P < 0.01$). VD₃ intervention substantially ameliorated these pathological changes,

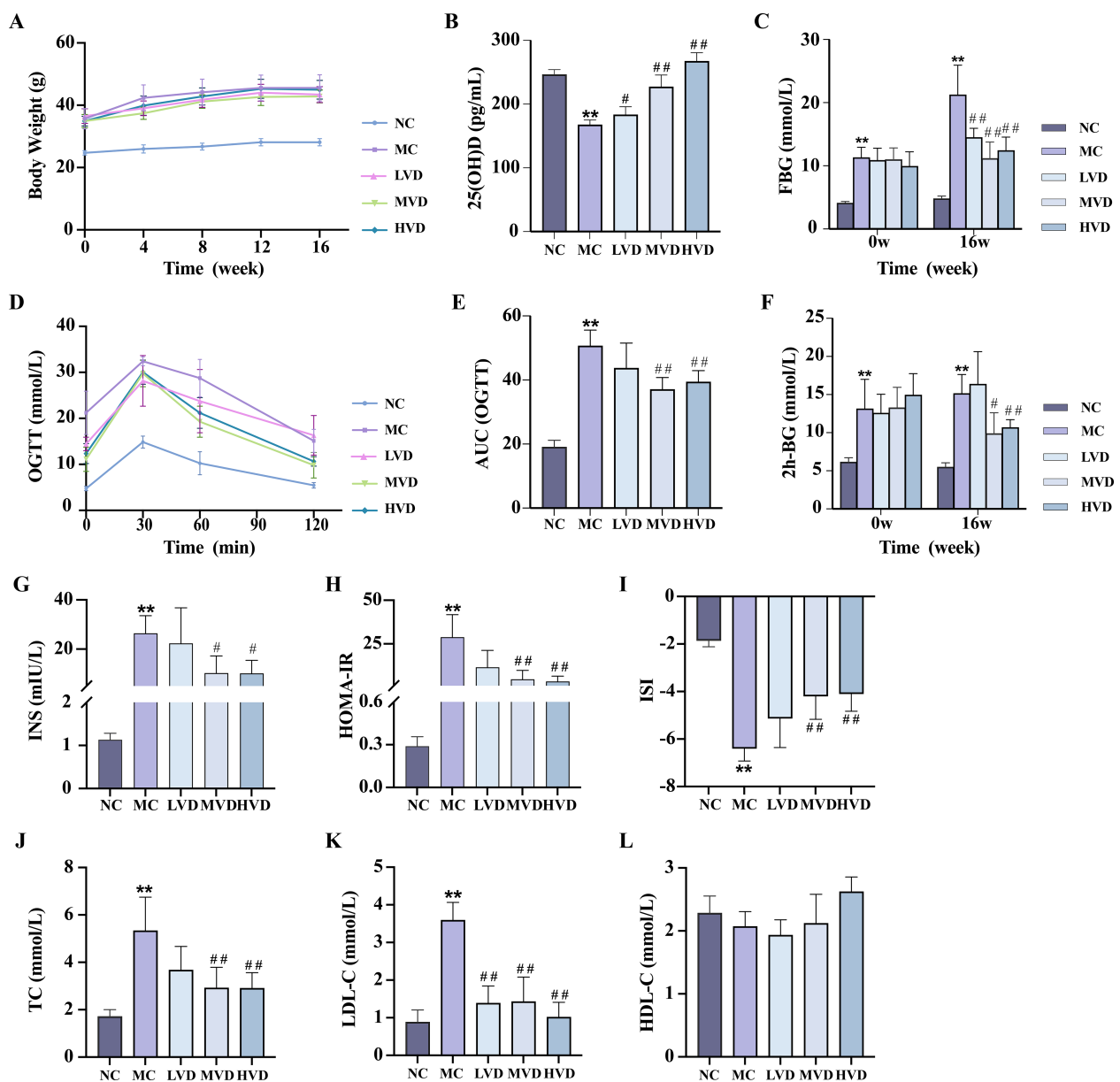


FIGURE 2

Effects of VD₃ supplementation on metabolic parameters in prediabetic mice. (A) Body weight (n=8). (B) Serum 25(OH)D levels (n=5). (C) FBG levels (n=8). (D, E) OGTT measurements and corresponding AUC (n=8). (F) 2h postprandial blood glucose levels (n=8). (G-I) Serum fasting insulin and respective insulin indices (n=3-10). (J-L) Serum TC, LDL-C, HDL-C levels (n=4). Data are presented as Mean \pm SD. * P < 0.05, ** P < 0.01, compared with the NC group; # P < 0.05, ## P < 0.01, compared with the MC group. FBG, fasting blood glucose; OGTT, oral glucose tolerance test; AUC, area under the curve; INS, fasting blood insulin; HOMA-IR, homeostasis model assessment of insulin resistance; ISI, insulin sensitivity index; TC, total cholesterol; TG, triglycerides; HDL-C, high-density lipoprotein cholesterol.

yielding improved myocardial histoarchitecture with reduced hypertrophy, fewer structural discontinuities, and better organized fiber arrangement (P < 0.01) (Figures 3A, B). Corresponding improvements were observed in echocardiographic parameters of ventricular structure and function. Additionally, VD₃ treatment significantly attenuated the elevated serum levels of cardiac injury markers CK and LDH observed in MC mice (P < 0.01) (Figures 3M, N). Collectively, these findings demonstrate that VD₃ intervention effectively mitigates both structural and functional cardiac abnormalities in prediabetic mice.

3.3 VD₃ supplementation attenuates cardiac ferroptosis in prediabetic mice

Prediabetic mice exhibited characteristic hyperglycemia and hyperlipidemia, metabolic disturbances known to promote excessive ROS generation and lipid peroxidation, ultimately leading to ferroptosis. Histochemical analyses revealed striking pathological alterations in cardiac tissues of MC group mice, including abundant ferric hemoflavin-containing particles, excessive lipid accumulation, and marked ROS deposition

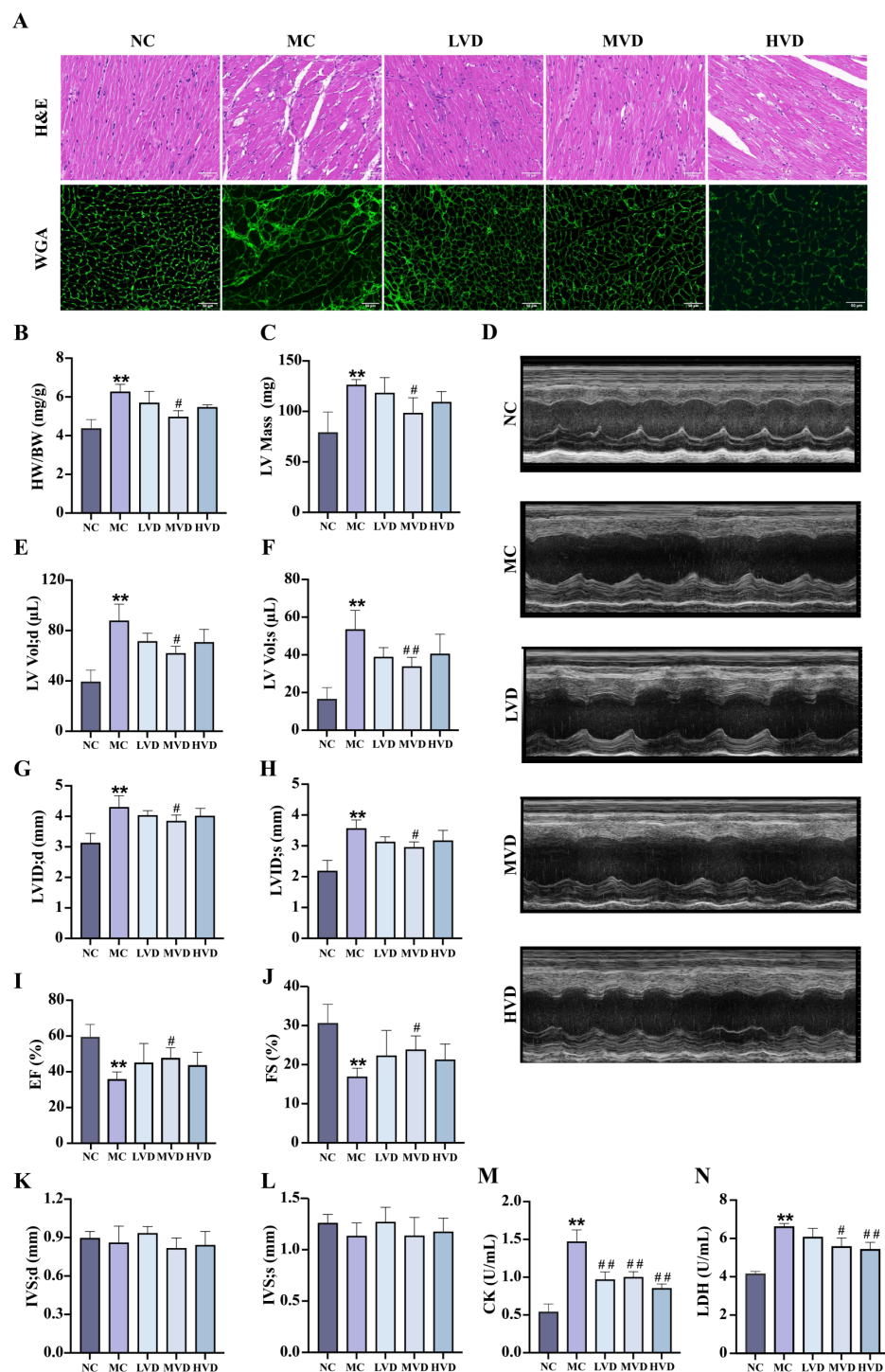


FIGURE 3

Effects of VD_3 supplementation on myocardial structure and function in prediabetic mice. (A) H&E and WGA staining ($n=3$), scale bar=50 μm . (B) The heart indexes ($n=3-6$). (C) LV mass ($n=5$). (D) Echocardiography images ($n=5$). (E-L) Echocardiographic parameters: LV Vol;d, LV Vol;s, LVID;d, LVID;s, EF%, FS%, IVS;d and IVS;s ($n=5$). (M) Serum CK levels ($n=6$). (N) Serum LDH levels ($n=6$). Data are presented as Mean \pm SD. * $P < 0.05$, ** $P < 0.01$, compared with the NC group; # $P < 0.05$, ## $P < 0.01$, compared with the MC group. CK, creatine kinase; LDH, lactate dehydrogenase.

(Figures 4A–C). These pathological features were significantly attenuated by VD_3 intervention ($P < 0.05$). The TUNEL assay confirmed increased cardiomyocyte death in MC mice, which was effectively mitigated by VD_3 treatment ($P < 0.05$). (Figures 4D, E). Quantitative assessments demonstrated that MC mice displayed

elevated cardiac iron content and MDA levels, coupled with depleted GSH reserves compared to NC group ($P < 0.01$) (Figures 4F–H). Western blot analysis further elucidated the molecular mechanisms underlying these observations: cardiac tissues from MC mice showed upregulated expression of

ferroptosis-promoting proteins (TFR1, ACSL4, NCOA4, and Ferritin), while exhibiting downregulation of the ferroptosis inhibitors SLC7A11 and GPX4 ($P < 0.01$) (Figures 4I–O). VD_3 intervention consistently reversed these expression patterns ($P < 0.05$). Collectively, these data demonstrate that ferroptosis contributes to cardiac pathology in prediabetic mice and that VD_3 administration exerts protective effects against this form of programmed cell death.

3.4 VD_3 supplementation suppresses ErbB4 and YAP activation in cardiac tissues of prediabetic mice

To further delineate the molecular mechanisms responsible for the cardioprotective effects of VD_3 , the expression of key signaling proteins in myocardial tissues were evaluated. Quantitative analysis revealed a significant upregulation of both NRG1 and phosphorylated ErbB4 (p-ErbB4) in MC mice compared to NC group ($P < 0.01$) (Figures 5A, B), an effect that was substantially attenuated following VD_3 intervention ($P < 0.05$). Notably, VD_3 treatment also induced a marked increase in phosphorylated YAP (p-YAP) levels, indicating effective activation of YAP ($P < 0.05$) (Figure 5C). Collectively, these findings demonstrate that VD_3 ameliorates prediabetic myocardial injury by downregulating NRG1 expression and subsequently affecting the activation of both ErbB4 and YAP signaling cascades.

3.5 Inhibition of ferroptosis alleviates HGPA-induced cardiomyocyte injury

To further elucidate the mechanisms underlying cardiomyocyte injury, an *in vitro* model was established using H9c2 cardiomyocytes exposed to HGPA. As depicted in supplementary Figure 1, exposure to a combination of 33.3 mM HG and 0.25 mM PA for 24h (designated as HGPA) significantly reduced cell viability ($P < 0.01$). Notably, pretreatment with 10 nM $1,25(OH)_2D_3$ for 2h remarkably enhanced cell viability followed by co-culture with HGPA for 24h ($P < 0.01$).

Subsequently, we explored whether inhibiting ferroptosis could alleviate cardiomyocyte injury induced by HGPA. *In vitro*, cells were initially exposed to 1 μ M Fer-1 for 2h, followed by co-incubation with HGPA for 24 h. A significant increase in the cross-sectional area was observed in HGPA+Fer-1 cells compared to HGPA group (Figures 6A, B). Additionally, the number of dead cells was notably decreased (Figures 6C, D), indicating a degree of recovery from damage. Furthermore, elevated levels of Fe^{2+} , MDA, and ROS, along with a substantial decrease in GSH levels, were detected in HGPA cells compared to normal cells (Figures 6E–I). Notably, these alterations were reversed upon application of the Fer-1. Western blot analysis was subsequently performed to assess key proteins implicated in ferroptosis. The results revealed a substantial upregulation in the relative expression levels of TFR1, ACSL4, and Ferritin, along with a notable reduction in the relative expression of SLC7A11 and GPX4 following HGPA exposure (Figures 6J–O). Intriguingly, these changes were reversed upon

treatment with the Fer-1. This study thus delineates the induction of ferroptosis in H9c2 cells by HGPA and highlights the potential of ferroptosis inhibition in mitigating HGPA-triggered cardiomyocyte injury.

3.6 Phospho-ErbB4 inhibitor modulates YAP-mediated ferroptosis and hypertrophy in H9c2 cardiomyocytes

During the progression of prediabetic myocardial injury, our investigations revealed concurrent ErbB4 activation, YAP activity suppression, and ferroptosis occurrence. To elucidate the precise interrelationship among these three factors, we conducted *in vitro* experiments involving pretreatment with 73.7 nM Dac for 2h followed by 24-h co-culture with HGPA to specifically inhibit ErbB4 phosphorylation and monitor subsequent changes. Comparative analysis demonstrated that Dac-treated cells exhibited significantly reduced cell mortality and markedly diminished cellular cross-sectional area (Figures 7A–D) relative to HGPA-treated cells. Western blot analysis confirmed effective ErbB4 phosphorylation inhibition (Figures 7E, F), which was accompanied by a substantial elevation in phosphorylated YAP levels (Figures 7G, H) and concurrent attenuation of ferroptosis markers (Figures 7I–S). Notably, the phosphorylation profiles of both ErbB4 and YAP showed no statistically significant differences between Fer-1-treated and Dac-treated groups. These collective findings establish a hierarchical relationship wherein ErbB4 operates upstream of YAP, and its reduced phosphorylation state appears to mitigate YAP-mediated ferroptotic processes in the context of prediabetic myocardial injury.

3.7 $1,25(OH)_2D_3$ inhibits ErbB4/YAP-dependent ferroptosis and attenuates myocardial injury

Our previous *in vivo* study demonstrated a decrease in p-ErbB4 expression following VD_3 intervention. Subsequently, we explored whether VD mitigates myocardial injury by modulating ErbB4/YAP-mediated ferroptosis. Therefore, *in vitro*, we added 10 nM $1,25(OH)_2D_3$ and 73.7 nM Dacomitinib for 2h pretreatment followed by 24h co-culture with HGPA [$1,25(OH)_2D_3$ +Dac]. Compared with HGPA group, HGPA+ $1,25(OH)_2D_3$ group showed a significant decrease in phosphorylated ErbB4 levels (Figure 8E), a significant increase in phosphorylated YAP levels (Figure 8F), and an inhibition of ferroptosis (Figures 8G–Q). Compared with HGPA + $1,25(OH)_2D_3$ group, the above indicators of HGPA+ $1,25(OH)_2D_3$ +Dac group were reversed more significantly, the cell cross-sectional area was significantly reduced (Figures 8A, B), and the number of dead cells was reduced (Figures 8C, D). The above analyses suggest that $1,25(OH)_2D_3$ inhibits ErbB4/YAP-mediated ferroptosis and rescues myocardial injury, and that p-ErbB4 inhibitor enhance the therapeutic effect of $1,25(OH)_2D_3$ on myocardial injury.

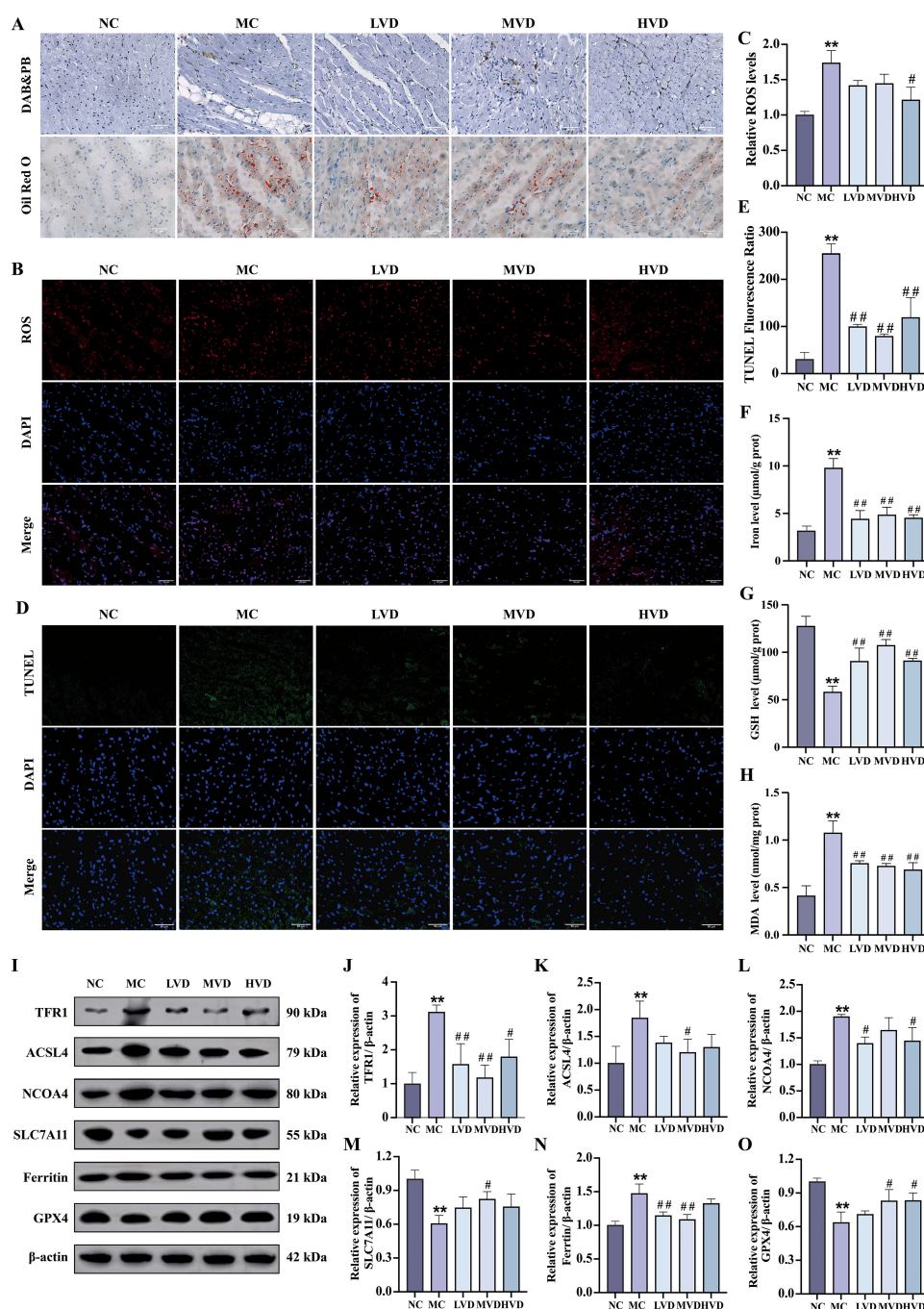


FIGURE 4

Effects of VD_3 supplementation on ferroptosis in prediabetic mice. (A) Images of Prussian blue & DAB and Oil Red O staining of hearts tissue ($n=3$), scale bar=50 μm . (B, C) Representative fluorescence images and quantitative analysis of ROS measurement ($n=3$). (D, E) Quantitative analysis of TUNEL fluorescence ratio in myocardial tissues ($n=3$), scale bar=50 μm . (F–H) Analysis of Fe^{2+} , GSH and MDA levels ($n=5$). (I–O) Representative western blot images and quantitative analysis of TFR1, ACSL4, NCOA4, SLC7A11, Ferritin and GPX4 protein expressions ($n=3$). Data are presented as Mean \pm SD. * $P < 0.05$, ** $P < 0.01$, compared with the NC group; # $P < 0.05$, ## $P < 0.01$, compared with the MC group. ROS, reactive oxygen species; GSH, glutathione; MDA, malondialdehyde; TFR1, transferrin receptor protein 1; ACSL4, acyl-CoA synthetase long chain family member 4; NCOA4, nuclear receptor coactivator 4; SLC7A11, solute carrier family 7 member 11; GPX4, glutathione peroxidase 4.

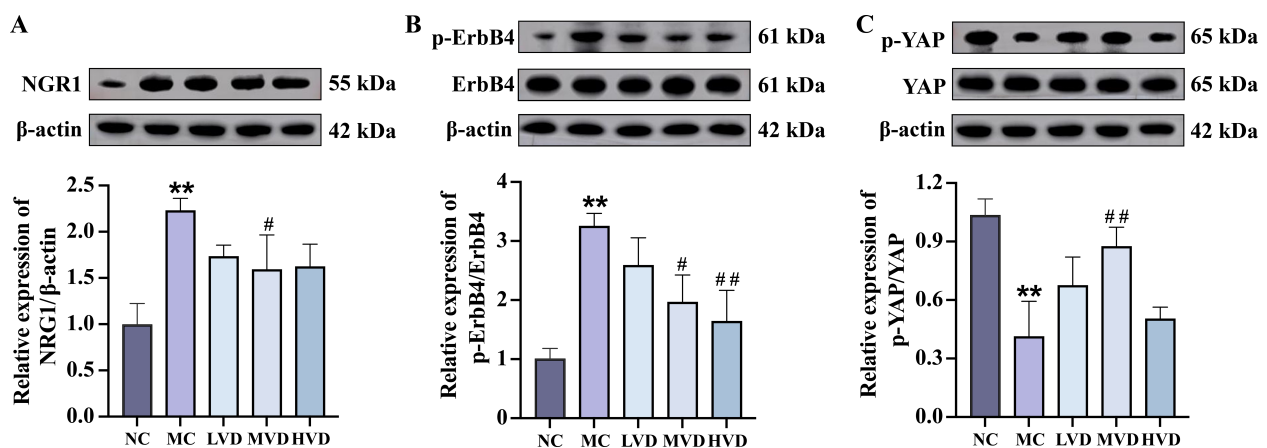


FIGURE 5

Effects of VD₃ supplementation on ErbB4 and YAP activation in cardiac tissues of prediabetic mice. (A–C) Representative western blot images and quantitative analysis of NRG1, phosphorylated ErbB4, and phosphorylated YAP (n=3). Data are presented as Mean ± SD. **P* < 0.05, ***P* < 0.01, compared with the NC group; #*P* < 0.05, ##*P* < 0.01, compared with the MC group. NRG1, neuregulin 1; ErbB4, receptor tyrosine-protein kinase erbB-4; YAP, yes-associated protein.

4 Discussion

Accumulating evidence indicates that cardiac injury initiates during the prediabetic stage (4, 5). Without timely intervention, this early injury may progress to diabetic cardiomyopathy - a distinct form of heart failure with potentially fatal consequences (1). The pathogenesis of diabetic cardiomyopathy is complex and multifactorial, and currently, no effective preventive or therapeutic strategies are available. Notably, observational studies have demonstrated an inverse correlation between serum 25(OH)D levels and cardiovascular risk in prediabetic patients (20). Additionally, VD status has been associated with cardiac autonomic function and metabolic regulation in prediabetes (21). These findings motivated our investigation into the cardioprotective effects of VD in prediabetic states, utilizing both *in vivo* and *in vitro* models.

The therapeutic potential of VD in prediabetes remains controversial. While some studies report that VD supplementation improves insulin sensitivity and reduces diabetes risk in VD-deficient prediabetic rodents, others have found no significant improvement in β-cell function indices following 24 months of VD₃ treatment in prediabetic patients (22–24). Our experimental data reveal that HFD-fed KKAY mice developed characteristic prediabetic features including hypovitaminosis D, hyperglycemia, dyslipidemia, glucose intolerance, insulin resistance, and obesity. Notably, a 16-week VD₃ intervention effectively ameliorated these metabolic disturbances, suggesting that VD₃ supplementation enhance insulin sensitivity and potentially delay diabetes onset in prediabetic individuals.

The cardiac pathology of diabetes spans structural abnormalities, functional impairments, and metabolic dysregulation (25, 26). In our study, echocardiographic analysis revealed that HFD-fed KKAY mice developed significant left ventricular dilation (increased volume and internal diameter), hypertrophy (increased mass), and systolic dysfunction (reduced EF and FS). These echocardiographic findings were corroborated by elevated serum cardiac enzymes (CK, LDH) and histopathological evidence of cardiomyocyte hypertrophy. VD₃

treatment significantly attenuated these pathological changes. These results are in line with clinical studies reporting that high-dose VD₃ supplementation can reduce left atrial enlargement and improve cardiovascular risk profiles in prediabetic patients (27, 28).

Our mechanistic investigation further revealed that KKAY mice exhibited increased myocardial ROS production and lipid peroxidation—hallmarks of ferroptosis (29, 30). Ferroptosis, an iron-dependent form of regulated cell death, has recently emerged as a promising therapeutic target in cardiovascular diseases, including diabetic cardiomyopathy (31, 32). Among oxidative stress biomarkers, GSH and MDA are widely recognized indicators of ferroptotic activity (33). GSH, the most abundant intracellular antioxidant, neutralizes lipid peroxides via the GPX4 pathway (34). Its depletion weakens cellular antioxidant defenses and is a defining feature of ferroptosis. Conversely, MDA, a reactive byproduct of lipid peroxidation, reflects oxidative damage to cellular membranes (35). In our model, prediabetic mice showed reduced myocardial GSH levels and elevated MDA levels, indicating ferroptosis and oxidative stress. Importantly, VD₃ treatment significantly restored GSH levels and decreased MDA accumulation, suggesting a protective effect of VD against oxidative stress-induced cardiomyocyte injury in prediabetic states. To functionally validate these findings, we used Ferrostatin-1, a specific ferroptosis inhibitor, in HGPA-treated H9c2 cardiomyocytes. Ferrostatin-1 effectively attenuated glycolipotoxicity-induced cardiomyocyte hypertrophy and cell death—findings consistent with previous reports by Wang et al. (32, 36). Moreover, while previous studies have shown that VD can regulate ferroptosis in various organs, including the heart, by inhibiting iron accumulation and lipid peroxidation (37–40), our data provide new evidence supporting a role for VD in modulating ferroptosis as a mechanism of cardioprotection in prediabetic models.

ErbB4, a key member of the EGFR family, is predominantly expressed in cardiac tissue and plays essential roles in cardiac development, physiological maintenance, as well as functions in the mammary gland and nervous system (41–43). Recent evidence has implicated ErbB4 in cardiac pathophysiology. For example, cardiac

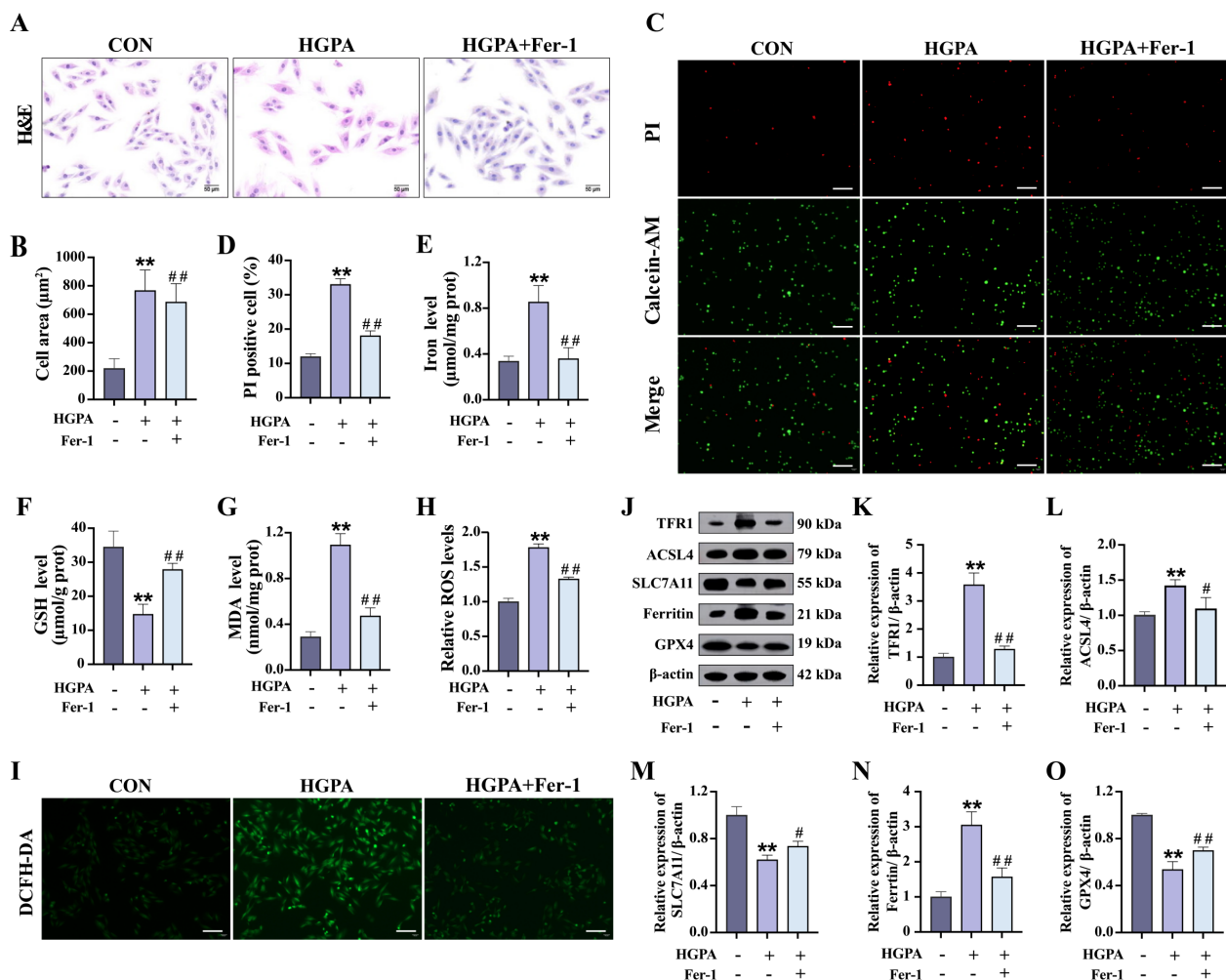


FIGURE 6

Effect of ferroptosis inhibition on HGPA-induced cardiomyocyte injury. (A–D) Myocardial hypertrophy and cell death status were assessed using images of H&E and PI/Calcein-AM staining ($n=3$), scale bar=50 μm . (E–G) Fe^{2+} , GSH and MDA levels in different groups ($n=6$). (H, I) Representative fluorescence images and quantitative analysis of DCFH-DA staining for ROS measurement in H9c2 cells ($n=3$), scale bar=50 μm . (J–O) Representative western blot images and quantitative analysis of TFR1, ACSL4, SLC7A11, Ferritin and GPX4 ($n=3$). Data are presented as Mean \pm SD. * $P < 0.05$, ** $P < 0.01$, compared with the CON group; # $P < 0.05$, ## $P < 0.01$, compared with the HGPA group. GSH, glutathione; MDA, malondialdehyde; ROS, reactive oxygen species; TFR1, transferrin receptor protein 1; ACSL4, acyl-CoA synthetase long chain family member 4; SLC7A11, solute carrier family 7 member 11; GPX4, glutathione peroxidase 4.

endothelial-specific ErbB4 deficiency has been shown to attenuate myocardial hypertrophy and fibrosis under stress (16), while ErbB4 activation can promote cardiomyocyte hypertrophy (15). In our study, cardiac tissue from HFD-induced KKAY mice displayed significant ErbB4 activation along with increased expression of its ligand, neuregulin-1 (NRG1). We found that this NRG1/ErbB4 signaling axis contributes to the development of myocardial hypertrophy during prediabetic cardiac injury. Furthermore, we observed activation of Yes-associated protein (YAP), a nuclear effector of the Hippo pathway, in these mice, which exhibited marked left ventricular dilation—a hallmark of hypertrophic remodeling. These observations are consistent with prior studies showing YAP's involvement in both compensatory hypertrophy following acute pressure overload (44) and pathological cardiac remodeling (45, 46). Importantly, VD_3 treatment effectively suppressed activation of both ErbB4 and YAP. This is in line with reports that VD analogs can bind ErbB4 (47) and modulate TGF-

β -induced YAP phosphorylation (48, 49). These findings suggest that VD's cardioprotective effects in prediabetes may, at least in part, be mediated via inhibition of the ErbB4/YAP signaling axis.

In our model, the MC group exhibited three key molecular changes: enhanced ErbB4 activation, suppressed YAP activity, and increased ferroptosis in cardiac tissues. Based on these observations, we hypothesized that ErbB4 signaling might serve as a regulatory node linking cardiac stress to ferroptosis during prediabetic injury. To test this, we conducted *in vitro* experiments using phospho-ErbB4 (p-ErbB4) and ferroptosis inhibitors in HGPA-treated H9c2 cells. Our results support a model in which ErbB4 acts upstream of YAP and potentially modulates ferroptosis by disrupting YAP-mediated signaling. Notably, treatment with $1,25(\text{OH})_2\text{D}_3$ mimicked the effects of p-ErbB4 inhibition, suppressing the ErbB4/YAP axis and reducing ferroptosis-related cellular injury. These *in vitro* findings further validate our *in vivo* results and suggest that VD may mitigate

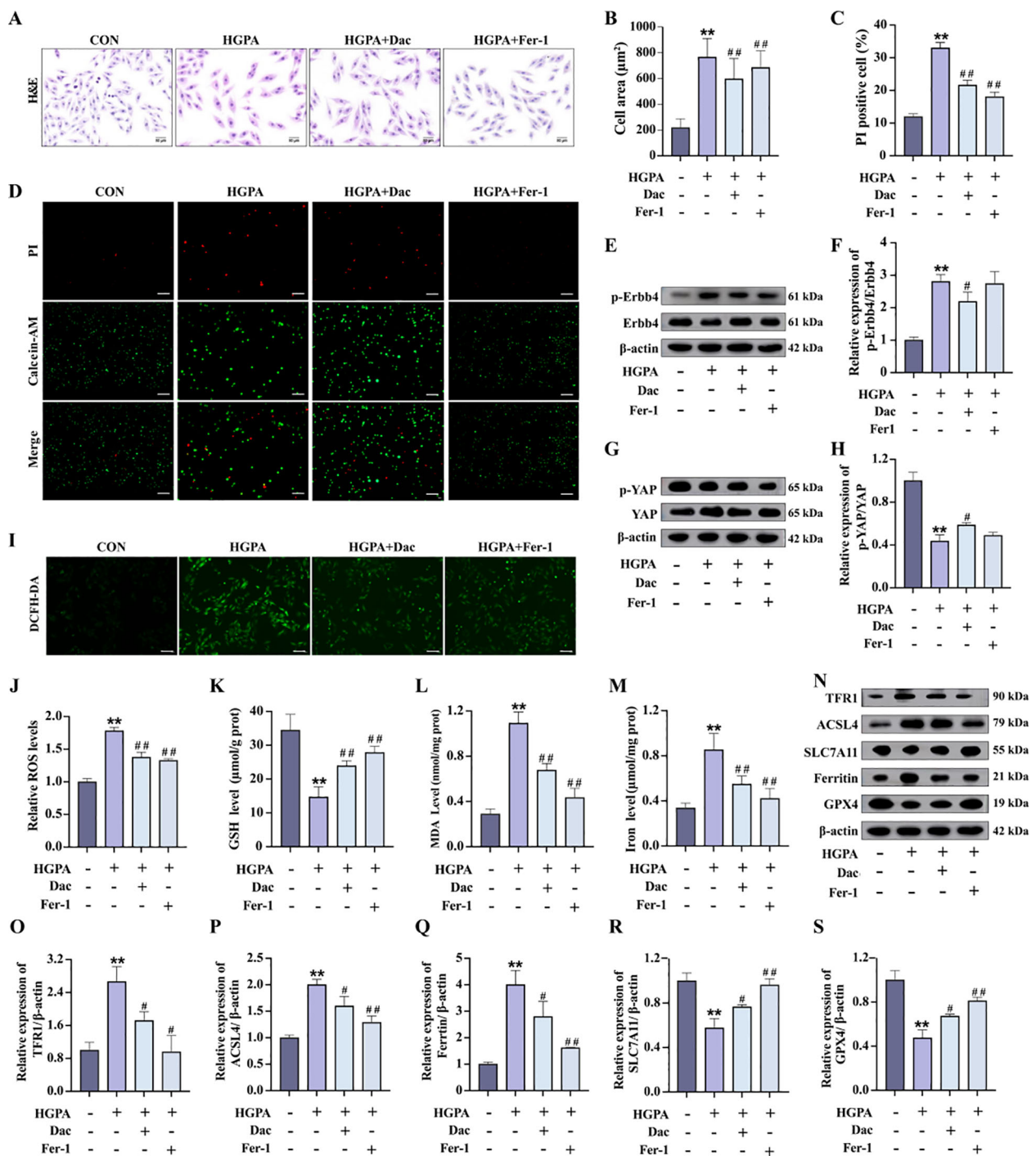


FIGURE 7

p-ErbB4 inhibitors regulate YAP-mediated ferroptosis in H9c2 cardiomyocytes. (A–D) Myocardial hypertrophy and cell death status were assessed by Images of H&E and PI staining (n=3), scale bar=50 μ m. (E–H) Representative western blot images and quantitative analysis of NRG1, phosphorylated ErbB4, and phosphorylated YAP (n=3). (I–J) Representative fluorescence images and quantitative analysis of DCFH-DA staining for ROS measurement in H9c2 cells (n=3), scale bar=50 μ m. (K–M) Analysis of Fe²⁺, GSH and MDA levels in H9c2 cells (n=6). (N–S) Representative western blot images and quantitative analysis of TFR1, ACSL4, SLC7A11, Ferritin and GPX4 (n=3). Data are presented as Mean \pm SD. * P < 0.05, ** P < 0.01, compared with the CON group; # P < 0.05, ## P < 0.01, compared with the HGPA group. ErbB4, receptor tyrosine-protein kinase erbB-4; YAP, yes-associated protein; GSH, glutathione; MDA, malondialdehyde; ROS, reactive oxygen species; TFR1, transferrin receptor protein 1; ACSL4, acyl-CoA synthetase long chain family member 4; SLC7A11, solute carrier family 7 member 11; GPX4, glutathione peroxidase 4.

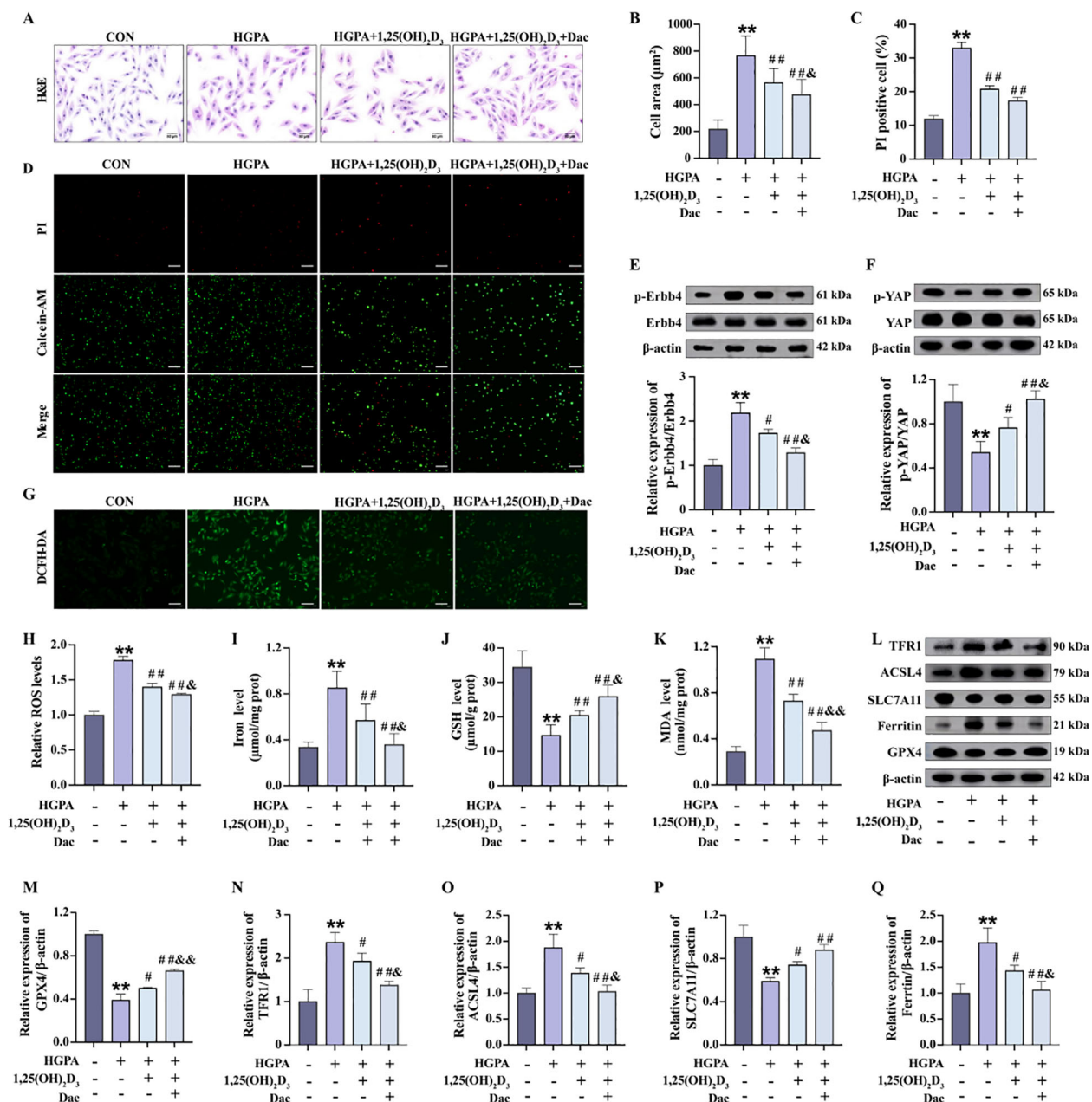


FIGURE 8

1,25(OH)₂D₃ inhibits ErbB4/YAP-mediated ferroptosis and rescues myocardial injury. (A–D) Myocardial hypertrophy and cell death status were assessed by images of H&E and PI staining (n=3), scale bar=50 μm. (E, F) Representative western blot images and quantitative analysis of NRG1, phosphorylated ErbB4, and phosphorylated YAP (n=3). (G, H) Representative fluorescence images and quantitative analysis of DCFH-DA staining for ROS measurement in H9c2 cells (n=3), scale bar=50 μm. (I–K) Analysis of Fe²⁺, GSH and MDA levels in H9c2 cells (n=6). (L–Q) Representative western blot images and quantitative analysis of TFR1, ACSL4, SLC7A11, Ferritin and GPX4 (n=3). Data are presented as Mean ± SD. **P* < 0.05, ***P* < 0.01, compared with the CON group; #*P* < 0.05, ##*P* < 0.01, compared with the HGPA group; [†]*P* < 0.05, ^{††}*P* < 0.01, compared with the HGPA +1,25(OH)₂D₃ group. ErbB4, receptor tyrosine-protein kinase erbB-4; YAP, yes-associated protein; GSH, glutathione; MDA, malondialdehyde; ROS, reactive oxygen species; TFR1, transferrin receptor protein 1; ACSL4, acyl-CoA synthetase long chain family member 4; SLC7A11, solute carrier family 7 member 11; GPX4, glutathione peroxidase 4.

prediabetic cardiac injury through modulation of the ErbB4/ferroptosis axis. The therapeutic relevance of this pathway is highlighted by the enhanced cardioprotective effects observed when combining 1,25(OH)₂D₃ with a p-ErbB4 inhibitor.

In summary, our study demonstrates that VD exerts beneficial effects on prediabetic cardiac injury. VD₃, the inactive precursor form, undergoes sequential hydroxylation—first in the

liver to form 25-hydroxyvitamin D₃ [25(OH)D₃], and then in the kidney to produce 1,25(OH)₂D₃, the biologically active form. We used VD₃ supplementation *in vivo* to assess systemic effects, and 1,25(OH)₂D₃ *in vitro* to directly probe cellular mechanisms. This dual approach enabled us to more precisely delineate the mechanistic basis of VD-mediated cardioprotection under prediabetic conditions.

Despite these promising findings, several limitations must be acknowledged. The *in vivo* environment is inherently complex, involving multiple interacting factors that may influence outcomes. Therefore, additional validation using population-based studies or ErbB4 knockdown/knockout animal models is necessary to confirm the proposed mechanisms. Moreover, our current investigation primarily focuses on the anti-hypertrophic effects of VD. Future studies should further explore its potential pharmacological impact on other pathological aspects of diabetic cardiomyopathy, including inflammation, myocardial fibrosis, and diastolic dysfunction.

5 Conclusions

Our study reveals for the first time the relationship between ErbB4 and ferroptosis in prediabetic cardiopathy, which provides novel evidence that VD can ameliorate diabetic cardiac injury, and that the combination of VD and p-ErbB4 inhibitor may be a feasible clinical strategy for treating prediabetic myocardial injuries.

Data availability statement

The raw data supporting the conclusions of this article will be made available by the authors, without undue reservation.

Ethics statement

The animal study was approved by Life Science Ethics Review Committee of Zhengzhou University (ZZUIRB2021-GZR0141). The study was conducted in accordance with the local legislation and institutional requirements.

Author contributions

YM: Conceptualization, Methodology, Writing – original draft. YZ: Project administration, Writing – review & editing. LZ: Investigation, Writing – review & editing. HC: Project administration, Writing – review & editing. LT: Project administration, Writing – review & editing. WL: Funding acquisition, Writing – review & editing. CG: Validation, Writing – review & editing. LL: Data curation, Writing – review & editing. XL: Writing – review & editing, Funding acquisition.

References

1. Dillmann WH. Diabetic cardiomyopathy. *Circ Res.* (2019) 124:1160–2. doi: 10.1161/CIRCRESAHA.118.314665
2. Wilson PW, D'Agostino RB, Parise H, Sullivan L, Meigs JB. Metabolic syndrome as a precursor of cardiovascular disease and type 2 diabetes mellitus. *Circulation.* (2005) 112:3066–72. doi: 10.1161/CIRCULATIONAHA.105.539528
3. Seferovic PM, Petrie MC, Filippatos GS, Anker SD, Rosano G, Bauersachs J, et al. Type 2 diabetes mellitus and heart failure: a position statement from the Heart Failure

HS: Writing – review & editing, Formal Analysis, Software, Conceptualization, Visualization.

Funding

The author(s) declare that financial support was received for the research and/or publication of this article. Work was supported by the National Natural Science Foundation of China [grant number 82173515, 82373568 and 82102562]; China Postdoctoral Science Foundation 73rd Batch General Project [grant number 2023M733206]; Henan Provincial Outstanding Youth Science Foundation [grant number 242300421080], and Scientific and Technological Innovation Programs of Higher Education Institutions in Shanxi (STIP) [grant number 2023L2224].

Conflict of interest

The authors declare that the research was conducted in the absence of any commercial or financial relationships that could be construed as a potential conflict of interest.

Generative AI statement

The author(s) declare that no Generative AI was used in the creation of this manuscript.

Publisher's note

All claims expressed in this article are solely those of the authors and do not necessarily represent those of their affiliated organizations, or those of the publisher, the editors and the reviewers. Any product that may be evaluated in this article, or claim that may be made by its manufacturer, is not guaranteed or endorsed by the publisher.

Supplementary material

The Supplementary Material for this article can be found online at: <https://www.frontiersin.org/articles/10.3389/fimmu.2025.1626295/full#supplementary-material>

Association of the European Society of Cardiology. *Eur J Heart Fail.* (2018) 20:853–72. doi: 10.1002/ehf.2018.20.issue-5

4. Nunes S, Soares E, Fernandes J, Viana S, Carvalho E, Pereira FC, et al. Early cardiac changes in a rat model of prediabetes: brain natriuretic peptide overexpression seems to be the best marker. *Cardiovasc Diabetol.* (2013) 12:44. doi: 10.1186/1475-2840-12-44

5. Koncsos G, Varga ZV, Baranyai T, Boengler K, Rohrbach S, Li L, et al. Diastolic dysfunction in prediabetic male rats: Role of mitochondrial oxidative

stress. *Am J Physiol Heart Circ Physiol.* (2016) 311:H927–h43. doi: 10.1152/ajpheart.00049.2016

6. Li X, Liu Y, Zheng Y, Wang P, Zhang Y. The effect of vitamin D supplementation on glycemic control in type 2 diabetes patients: A systematic review and meta-analysis. *Nutrients.* (2018) 10(3):375. doi: 10.3390/nu10030375

7. Zhang Y, Xue Y, Zhang D, Liu Y, Xu Z, Gao J, et al. Effect of vitamin D supplementation on glycemic control in prediabetes: A meta-analysis. *Nutrients.* (2021) 13(12):4464. doi: 10.3390/nu13124464

8. Harris E. Meta-analysis: vitamin D therapy reduced type 2 diabetes. *Jama.* (2023) 329:703. doi: 10.1001/jama.2023.1550

9. Lee TW, Kao YH, Chen YJ, Chao TF, Lee TI. Therapeutic potential of vitamin D in AGE/RAGE-related cardiovascular diseases. *Cell Mol Life Sci.* (2019) 76:4103–15. doi: 10.1007/s00018-019-03204-3

10. Guo X, Lin H, Liu J, Wang D, Li D, Jiang C, et al. 1,25-Dihydroxyvitamin D attenuates diabetic cardiac autophagy and damage by vitamin D receptor-mediated suppression of FoxO1 translocation. *J Nutr Biochem.* (2020) 80:108380. doi: 10.1016/j.jnutbio.2020.108380

11. Derakhshanian H, Djazayeri A, Javanbakht MH, Eshraghian MR, Mirshafiey A, Jahanabadi S, et al. Vitamin D downregulates key genes of diabetes complications in cardiomyocyte. *J Cell Physiol.* (2019) 234:21352–8. doi: 10.1002/jcp.v234.11

12. Marwick TH, Ritchie R, Shaw JE, Kaye D. Implications of underlying mechanisms for the recognition and management of diabetic cardiomyopathy. *J Am Coll Cardiol.* (2018) 71:339–51. doi: 10.1016/j.jacc.2017.11.019

13. Dhalla NS, Shah AK, Tappia PS. Role of oxidative stress in metabolic and subcellular abnormalities in diabetic cardiomyopathy. *Int J Mol Sci.* (2020) 21(7):2413. doi: 10.3390/ijms21072413

14. Chen Y, Hua Y, Li X, Arslan IM, Zhang W, Meng G. Distinct types of cell death and the implication in diabetic cardiomyopathy. *Front Pharmacol.* (2020) 11:42. doi: 10.3389/fphar.2020.00042

15. Wang Z, Chan HW, Gambarotta G, Smith NJ, Purdue BW, Pennisi DJ, et al. Stimulation of the four isoforms of receptor tyrosine kinase ErbB4, but not ErbB1, confers cardiomyocyte hypertrophy. *J Cell Physiol.* (2021) 236:8160–70. doi: 10.1002/jcp.v236.12

16. Dugaucquier L, Feyen E, Mateu L, Bruyns TAM, De Keulenaer GW, Segers VFM. The role of endothelial autocrine NRG1/ERBB4 signaling in cardiac remodeling. *Am J Physiol Heart Circ Physiol.* (2020) 319:H443–h55. doi: 10.1152/ajpheart.00176.2020

17. Lee C, Kim M, Park C, Jo W, Seo JK, Kim S, et al. Epigenetic regulation of Neuregulin 1 promotes breast cancer progression associated to hyperglycemia. *Nat Commun.* (2023) 14:439. doi: 10.1038/s41467-023-36179-8

18. Poursaitidis I, Wang X, Crighton T, Labuschagne C, Mason D, Cramer SL, et al. Oncogene-selective sensitivity to synchronous cell death following modulation of the amino acid nutrient cystine. *Cell Rep.* (2017) 18:2547–56. doi: 10.1016/j.celrep.2017.02.054

19. Wang C, Zeng J, Li LJ, Xue M, He SL. Cdc25A inhibits autophagy-mediated ferroptosis by upregulating ErbB2 through PKM2 dephosphorylation in cervical cancer cells. *Cell Death Dis.* (2021) 12:1055. doi: 10.1038/s41419-021-04342-y

20. Cao YB, Wei D, Yang LX, Luo ZJ, Yu PW, Li H, et al. Nanoplatform self-assembly from small molecules of porphyrin derivatives for NIR-II fluorescence imaging guided photothermal-immunotherapy. *Advanced Healthcare Materials.* (2022) 11(11):e2102526. doi: 10.21203/rs.3.rs-855967/v1

21. Dimova R, Chakarova N, Kirilov G, Grozeva G, Shinkov A, Tankova T. Vitamin D binding protein is related to cardiac autonomic function and metabolic status in prediabetes. *Nutr Res.* (2020) 75:56–66. doi: 10.1016/j.nutres.2019.12.008

22. Rasouli N, Brodsky IG, Chatterjee R, Kim SH, Pratley RE, Staten MA, et al. Effects of vitamin D supplementation on insulin sensitivity and secretion in prediabetes. *J Clin Endocrinol Metab.* (2022) 107:230–40. doi: 10.1210/clinem/dgab649

23. Niroomand M, Fotouhi A, Irannejad N, Hosseiniapanah F. Does high-dose vitamin D supplementation impact insulin resistance and risk of development of diabetes in patients with pre-diabetes? A double-blind randomized clinical trial. *Diabetes Res Clin Pract.* (2019) 148:1–9. doi: 10.1016/j.diabres.2018.12.008

24. Krisnamurti DGB, Louisa M, Poerwaningsih EH, Tarigan TJE, Soetikno V, Wibowo H, et al. Vitamin D supplementation alleviates insulin resistance in prediabetic rats by modifying IRS-1 and PPAR γ /NF- κ B expressions. *Front Endocrinol (Lausanne).* (2023) 14:1089298. doi: 10.3389/fendo.2023.1089298

25. Yancy CW, Jessup M, Bozkurt B, Butler J, Casey DE Jr., Drazner MH, et al. 2013 ACCF/AHA guideline for the management of heart failure: a report of the American College of Cardiology Foundation/American Heart Association Task Force on practice guidelines. *Circulation.* (2013) 128:e240–327. doi: 10.1161/CIR.0b013e31829e8776

26. Jia G, DeMarco VG, Sowers JR. Insulin resistance and hyperinsulinaemia in diabetic cardiomyopathy. *Nat Rev Endocrinol.* (2016) 12:144–53. doi: 10.1038/nrendo.2015.216

27. Desouza C, Chatterjee R, Vickery EM, Nelson J, Johnson KC, Kashyap SR, et al. The effect of vitamin D supplementation on cardiovascular risk in patients with prediabetes: A secondary analysis of the D2d study. *J Diabetes Complications.* (2022) 36:108230. doi: 10.1016/j.jdiacomp.2022.108230

28. Chacko SJ, Pauwaa S, Barends E, Ciubotaru I, Kansal MM. Vitamin D attenuates left atrial volume changes in african american males with obesity and prediabetes. *Echocardiography.* (2016) 33:681–5. doi: 10.1111/echo.2016.33.issue-5

29. Zhang S, Liu X, Wang J, Yuan F, Liu Y. Targeting ferroptosis with miR-144-3p to attenuate pancreatic β cells dysfunction via regulating USP22/SIRT1 in type 2 diabetes. *Diabetol Metab Syndr.* (2022) 14:89. doi: 10.1186/s13098-022-00852-7

30. Alka K, Mohammad G, Kowluru RA. Regulation of serine palmitoyl-transferase and Rac1-Nox2 signaling in diabetic retinopathy. *Sci Rep.* (2022) 12:16740. doi: 10.1038/s41598-022-20243-2

31. Wu X, Li Y, Zhang S, Zhou X. Ferroptosis as a novel therapeutic target for cardiovascular disease. *Theranostics.* (2021) 11:3052–9. doi: 10.7150/thno.54113

32. Wang X, Chen X, Zhou W, Men H, Bao T, Sun Y, et al. Ferroptosis is essential for diabetic cardiomyopathy and is prevented by sulforaphane via AMPK/NRF2 pathways. *Acta Pharm Sin B.* (2022) 12:708–22. doi: 10.1016/j.apsb.2021.10.005

33. Ayala A, Muñoz MF, Argüelles S. Lipid peroxidation: production, metabolism, and signaling mechanisms of malondialdehyde and 4-hydroxy-2-nonenal. *Oxid Med Cell Longev.* (2014) 2014:360438. doi: 10.1155/2014/360438

34. Yang WS, Stockwell BR. Ferroptosis: death by lipid peroxidation. *Trends Cell Biol.* (2016) 26:165–76. doi: 10.1016/j.tcb.2015.10.014

35. Conrad M, Pratt DA. The chemical basis of ferroptosis. *Nat Chem Biol.* (2019) 15:1137–47. doi: 10.1038/s41589-019-0408-1

36. Wu Y, Huang T, Li X, Shen C, Ren H, Wang H, et al. Retinol dehydrogenase 10 reduction mediated retinol metabolism disorder promotes diabetic cardiomyopathy in male mice. *Nat Commun.* (2023) 14:1181. doi: 10.1038/s41467-023-36837-x

37. Cai Y, Li X, Tan X, Wang P, Zhao X, Zhang H, et al. Vitamin D suppresses ferroptosis and protects against neonatal hypoxic-ischemic encephalopathy by activating the Nrf2/HO-1 pathway. *Transl Pediatr.* (2022) 11:1633–44. doi: 10.21037/tp-22-397

38. Liu X, Wang S, Jin S, Huang S, Liu Y. Vitamin D(3) attenuates cisplatin-induced intestinal injury by inhibiting ferroptosis, oxidative stress, and ROS-mediated excessive mitochondrial fission. *Food Funct.* (2022) 13:10210–24. doi: 10.1039/D2FO01028C

39. Cheng K, Huang Y, Wang C. 1,25(OH)(2)D(3) inhibited ferroptosis in zebrafish liver cells (ZFL) by regulating keap1-nrf2-GPx4 and NF- κ B-hepcidin axis. *Int J Mol Sci.* (2021) 22(21):11334. doi: 10.3390/ijms222111334

40. Hu Z, Zhang H, Yi B, Yang S, Liu J, Hu J, et al. VDR activation attenuate cisplatin induced AKI by inhibiting ferroptosis. *Cell Death Dis.* (2020) 11:73. doi: 10.1038/s41419-020-2256-z

41. Qiu C, Tarrant MK, Choi SH, Sathyamurthy A, Bose R, Banjade S, et al. Mechanism of activation and inhibition of the HER4/ErbB4 kinase. *Structure.* (2008) 16:460–7. doi: 10.1016/j.str.2007.12.016

42. Segers VFM, Dugaucquier L, Feyen E, Shakeri H, De Keulenaer GW. The role of ErbB4 in cancer. *Cell Oncol (Dordr).* (2020) 43:335–52. doi: 10.1007/s13402-020-00499-4

43. Icli B, Bharti A, Pentassuglia L, Peng X, Sawyer DB. ErbB4 localization to cardiac myocyte nuclei, and its role in myocyte DNA damage response. *Biochem Biophys Res Commun.* (2012) 418:116–21. doi: 10.1016/j.bbrc.2011.12.144

44. Kashiwara T, Mukai R, Oka SI, Zhai P, Nakada Y, Yang Z, et al. YAP mediates compensatory cardiac hypertrophy through aerobic glycolysis in response to pressure overload. *J Clin Invest.* (2022) 132(6):e150595. doi: 10.1172/JCI150595

45. Yue P, Zhang Y, Liu L, Zhou K, Xia S, Peng M, et al. Yap1 modulates cardiomyocyte hypertrophy via impaired mitochondrial biogenesis in response to chronic mechanical stress overload. *Theranostics.* (2022) 12:7009–31. doi: 10.7150/thno.74563

46. Wu W, Ziemann M, Huynh K, She G, Pang ZD, Zhang Y, et al. Activation of Hippo signaling pathway mediates mitochondria dysfunction and dilated cardiomyopathy in mice. *Theranostics.* (2021) 11:8993–9008. doi: 10.7150/thno.62302

47. SN B, KK P, Akey KS, Sankaran S, Raman RK, Natarajan J, et al. Vitamin D analog calcitriol for breast cancer therapy: an integrated drug discovery approach. *J Biomol Struct Dyn.* (2023) 41:11017–43. doi: 10.1080/07391102.2023.2199866

48. Wang D, Lin L, Lei K, Zeng J, Luo J, Yin Y, et al. Vitamin D3 analogue facilitates epithelial wound healing through promoting epithelial-mesenchymal transition via the Hippo pathway. *J Dermatol Sci.* (2020) 100:120–8. doi: 10.1016/j.jdermsci.2020.08.015

49. Sun Q, Gao Y, Qiao L, Yuan Y, Liu Q. 25(OH)-Vitamin D alleviates neonatal infectious pneumonia via regulating TGF β -mediated nuclear translocation mechanism of YAP/TAZ. *Bioengineered.* (2021) 12:8931–42. doi: 10.1080/21655979.2021.1990000